

Soft Material Characterization for Robotic Applications

Jennifer C. Case, Edward L. White, and Rebecca K. Kramer

Abstract

In this article we present mechanical measurements of three representative elastomers used in soft robotic systems: Sylgard 184, Smooth-Sil 950, and EcoFlex 00-30. Our aim is to demonstrate the effects of the nonlinear, time-dependent properties of these materials to facilitate improved dynamic modeling of soft robotic components. We employ uniaxial pull-to-failure tests, cyclic loading tests, and stress relaxation tests to provide a qualitative assessment of nonlinear behavior, batch-to-batch repeatability, and effects of prestraining, cyclic loading, and viscoelastic stress relaxation. Strain gauges composed of the elastomers embedded with a microchannel of conductive liquid (eutectic gallium–indium) are also tested to quantify the interaction between material behaviors and measured strain output. It is found that all of the materials tested exhibit the Mullins effect, where the material properties in the first loading cycle differ from the properties in all subsequent cycles, as well as response sensitivity to loading rate and production variations. Although the materials tested show stress relaxation effects, the measured output from embedded resistive strain gauges is found to be uncoupled from the changes to the material properties and is only a function of strain.

Introduction

SOFT ROBOTS HAVE THE POTENTIAL to change the way we construct intelligent systems. By using highly deformable and stretchable materials, we can build robots that safely interact with human operators and function in unstructured environments such as debris fields or within the human body. To date, various types of soft robotic components have been demonstrated, including resistance-based sensors,^{1–4} capacitance-based sensors,^{5–7} ionic actuators,^{8–10} pneumatic actuators,^{11–14} and dielectric actuators.^{15–17} Recent work on soft sensing technologies has employed liquid-metal-embedded elastomers to measure surface strain,^{1,2,18} joint angles,^{19,20} and applied pressure.^{4,21} These sensor devices rely on deformations of elastomers, including two of the elastomers we analyze in this work, to produce a change in resistance in embedded liquid metal.

In order to advance the field of soft robotics, additional knowledge of material behavior is needed. This knowledge will facilitate the design of soft robotic structures and will provide the basis for control of soft-bodied systems. It should be noted that our work does not set out to rigorously characterize and model non-linear and viscoelastic elastomers,^{22–28} but rather provides a practical guide to material selection for the soft robotics community. Linear and time-invariant material models do not account for many of the dynamics observed in soft systems. Recent work by Overveld *et al.* has started to

address this deficiency by investigating soft strain sensors undergoing large deformations.²⁹ However, the prior work did not include measurements or consideration of the time-dependent properties of soft materials. To our knowledge, this effect has not been rigorously evaluated in the soft robotics literature. To develop models that predict the response of soft materials over extended time scales, measurements of time-dependent material responses are required.

Furthermore, elastomers of the type commonly used in soft robots typically exhibit variability in material properties between nominally equivalent batches (batch-to-batch variability), which further complicates the modeling of material properties. This effect is particularly acute when developing control algorithms for soft robots, where variability in material properties will drive variability in plant dynamics. Control systems must be robust to this variability in order to achieve effective control.

In this article, we present our studies on the mechanical and resistive properties of three elastomers we have used to create soft robotic devices: Sylgard 184,^{5,20} Smooth-Sil 950, and EcoFlex 00-30.^{1,2} From these materials, we created two different types of test samples. The first type of sample is a homogeneous elastomeric “dog bone” used in stress–strain testing. The second type of sample is a liquid-metal-embedded elastomeric strain gauge, used to determine the interaction between the material properties and the output of

a soft resistive sensor. Our experiments are designed to provide a qualitative assessment on five critical areas: nonlinear behavior, batch-to-batch repeatability, effects of pre-straining, cyclic loading, and viscoelastic stress relaxation.

Previous work

Elastomers have been well studied and many of the unique properties of the materials are well known.^{30,31} Although no general theory exists to predict complete viscoelastic elastomeric behavior *a priori*, progress has been made describing certain aspects of elastomeric behavior. Beginning in the 1940s, Mullins identified an effect in natural rubber whereby straining the rubber resulted in a weakening.³² Later groups have extended this to other rubber-like materials, suggesting that it is in fact a common effect among all cross-linked elastomers, as summarized in the review by Diani *et al.*³³ In addition to nonlinear behaviors, elastomers are also susceptible to viscoelastic creep and stress relaxation. Many models have been proposed to capture the effects of viscoelastic materials, including the two-element Maxwell and Kelvin models, and the serial combination of the two called the Burgers model.³⁴ The Zener model is a modified Kelvin model with an additional spring.³⁵

Further complicating matters, actual properties differ from nominal properties due to variations in material processing, such as the cure temperature and base elastomer-to-curing agent ratio.³¹ As a result of these complexities, there is a wide range of material properties reported in the literature. One reference lists values for the Young's modulus of polydimethylsiloxane, of which Sylgard 184 is one formulation, spanning a full order of magnitude (360–3000 kPa).³⁶

Of the three materials we are studying, Sylgard 184 is by far the most represented in the literature. For example, Schneider *et al.* published a study of the stress–strain relationship of Sylgard 184 under different temperature conditions and with different compositions.³⁰ They limited their analysis mostly to the linear region of the stress–strain curve, which is generally below 40% strain. The two other materials we considered have not yet been described to this extent in the literature. Additionally, the available soft robotics literature does not address the time-dependent nature of these elastomeric materials.

Material deformation model

In the following sections, we develop the analytical models used in this work. Due to the large strains present in our elastomeric samples, our results are presented in terms of true stress, rather than engineering stress. This difference takes into account the reduction in cross-sectional area during the test. We assume a Poisson's ratio $\nu = 0.5$ in all of our calculations, as is generally done with rubber-like materials. This assumption is identical to assuming conservation of volume during the test. Assuming that the material is isotropic, and using the differential form of Poisson's ratio with no assumptions on linearity, we find the cross-sectional area as a function of extension to be

$$A = WT(1 - 2\delta + \delta^2) \quad (1a)$$

$$\delta = 1 - \left(1 + \frac{\Delta L}{L}\right)^{-\nu} \quad (1b)$$

where A is the resulting cross-sectional area, and δ represents the contraction normal to the direction of stretching. Note that ΔL is the corrected length with correction factor applied described later, not the applied extension.

Material relaxation models

The Maxwell, Zener, and Burgers models of viscoelastic relaxation are shown in Figure 1. The Maxwell model estimates the time evolution of the stress in a relaxing viscoelastic material. The model is presented below in Equation 2.²⁷

$$\sigma = \varepsilon R e^{-Rt/\eta} \quad (2)$$

where σ is stress, ε is strain, R is the spring constant, η is the damping coefficient, and t is time. The Zener model is presented below in Equation 3.²⁸

$$\sigma = \varepsilon \left(R_1 + R_2 e^{-\frac{R_2(R_1 + R_2)t}{R_1\eta}} \right) \quad (3)$$

where R_1 is the parallel spring constant, R_2 is the serial spring constant, and η is the damping coefficient. The Burgers model is presented below in Equation 4.²⁷

$$\sigma = \varepsilon \frac{(q_1 - q_2 r_1) e^{-r_1 t} - (q_1 - q_2 r_2) e^{-r_2 t}}{A} \quad (4a)$$

$$p_1 = \frac{\eta_1}{R_1} + \frac{\eta_1}{R_2} + \frac{\eta_2}{R_2}, p_2 = \frac{\eta_1 \eta_2}{R_1 R_2} \quad (4b)$$

$$q_1 = \eta_1, q_2 = \frac{\eta_1 \eta_2}{R_2} \quad (4c)$$

$$r_1, r_2 = \frac{p_1 \mp A}{2p_2} \quad (4d)$$

$$A = \sqrt{p_1^2 - 4p_2} \quad (4e)$$

where η_1 is the serial damping coefficient, η_2 is the parallel damping coefficient, R_1 is the serial spring constant, R_2 is the parallel spring constant, and $p_1, p_2, q_1, q_2, r_1, r_2$, and A are

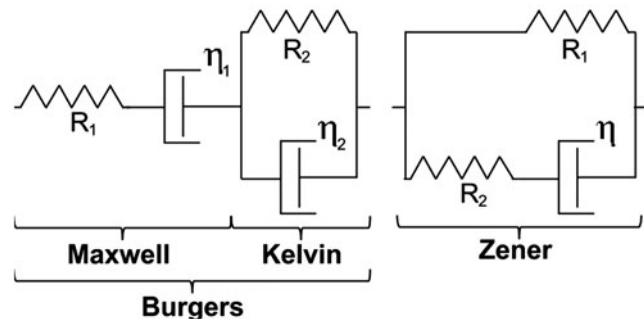


FIG. 1. Models of viscoelastic creep.

intermediate variables. As we noted above in the discussion of nonlinear properties, there is no model to predict the coefficients of the models without resorting to experiments. Equations 2–4 were used to model the time-dependent viscoelastic creep of the elastomers as described below.

Resistive strain gauge model

The strain gauges used in this study utilize liquid metal (eutectic gallium–indium)-filled microchannels in an elastomeric substrate.^{2,37} As the gauge strains, the length and cross-sectional area of the microchannels change, resulting in a change in resistance of the liquid metal. Our analytical model of the liquid-metal-embedded elastomeric strain gauges is based on several assumptions. First, we assume that all of the strain in the gauge is parallel to the direction of the microchannels. This assumption is justified since the bulk of the strain gauge is in the center of the dog-bone sample, where stress and strain are nearly uniaxial. Second, we neglect all of the parts of the sensor that are not part of the primary linear pattern. This includes the channels to the bonding ports and the semicircles at the top and bottom of the channels. This assumption is justified since the lengths that we are neglecting are small compared to the “active” length of the device. Finally, we assume that the liquid metal contained in the sensor is incompressible. With this, we can say that the volume of liquid metal in the strain gauge is

$$V = 4L_0A_0 = 4LA \quad (5)$$

where V is the volume of the liquid metal, L_0 is the initial length, A_0 is the initial area, L is a deformed length, A is a deformed area, and the coefficient accounts for the presence of four parallel channels in the strain gauge. Thus,

$$A = \frac{4L_0A_0}{4L} = \frac{L_0A_0}{L_0 + \delta} = \frac{A_0}{1 + \epsilon} \quad (6)$$

where δ is the deformation and $\epsilon = \frac{\delta}{L_0}$ is the strain. Further, the resistance of the strain gauge is

$$R = \frac{\rho L}{A} \quad (7)$$

Combining Equations 6 and 7 results in the ratio of change in resistance to initial resistance, which is the expression we compare to experimental results:

$$\frac{\Delta R}{R_0} = \epsilon(2 + \epsilon) \quad (8)$$

Materials and Methods

The three elastomers described in this article were all prepared using similar processes. All of these elastomers are delivered as two liquid or paste parts that were mixed together to begin crosslinking. The two liquid parts were massed using a Brecknell MBS-6000 electronic balance with 0.1 g resolution. These parts were mixed using a THINKY ARE-310 centrifugal mixer. The uncured liquid elastomer was spun onto cleaned 3"×2" glass slides using a Specialty Coating Systems Spincoat G3-8 spin coater. All of the sam-

ples were spun for 60 s, with 10 s acceleration and deceleration periods. The EcoFlex 00-30 and Sylgard 184 were both spun at 200 RPM, resulting in thickness of $371.4 \pm 31.85 \mu\text{m}$ and $307.6 \pm 19.63 \mu\text{m}$, respectively. Smooth-Sil 950 was spun at 400 RPM, resulting in a thickness of $643.0 \pm 40.57 \mu\text{m}$. The thickness measurements were obtained using a Zeta Instruments Zeta-20 True Color 3D Optical Profiler after curing and patterning, described below.

Samples for material testing and blank slides to be patterned into strain gauges were placed into an incubator set to 60°C to cure overnight. Once cured, elastomeric films were patterned using a Universal Laser Systems VLS 230, utilizing a 10.6 μm CO₂ laser. All of the material testing experiments (i.e., all experiments without embedded strain gauges) used the same material sample geometry, which is shown in Figure 2a. The geometry is specified in inches to maintain compatibility with the laser drivers. Six patterns of this design can be cut from a single substrate.

In order to fabricate the liquid-metal-embedded strain gauges, two layers of elastomer were utilized. The fabrication sequence consists of patterning a bottom layer of elastomer with microfluidic channels, as seen in Figure 2b, bonding an upper layer of elastomer to close the channels, injecting liquid gallium–indium alloy into the channels, inserting wires into the parts for electrical connectivity, and finally sealing the wires in place. In the case of Sylgard 184 and Smooth-Sil 950, the first step in the fabrication of a strain gauge was to pattern a blank slide of elastomer. These are the same slides used to fabricate material test samples described above. To pattern these slides, the same laser system is used, but with lower power to achieve a controlled partial cut into the material. Once patterned and cleaned, another slide with spin-coated elastomer was partially cured until tacky. The patterned elastomeric sheet was then pressed into this tacky layer with the microchannels between the two layers to achieve a bond between the two layers. In the case of EcoFlex 00-30, we utilized an SU-8 mold on a glass slide to pattern the material. Once cured, the patterned EcoFlex 00-30 sheet was bonded to an unpatterned sheet of equal thickness using oxygen plasma in a PlasmaEtch PE-50. Four-terminal measurements were used for these sensors to negate the effect of contact and interface resistances.

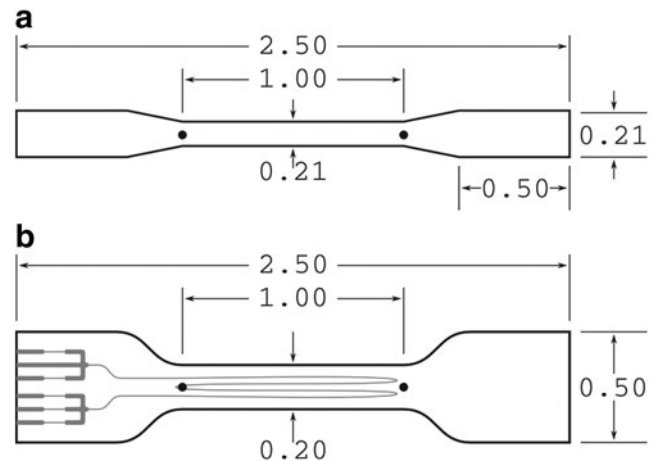


FIG. 2. Test sample geometry for (a) elastomeric dog bones and (b) strain sensors.

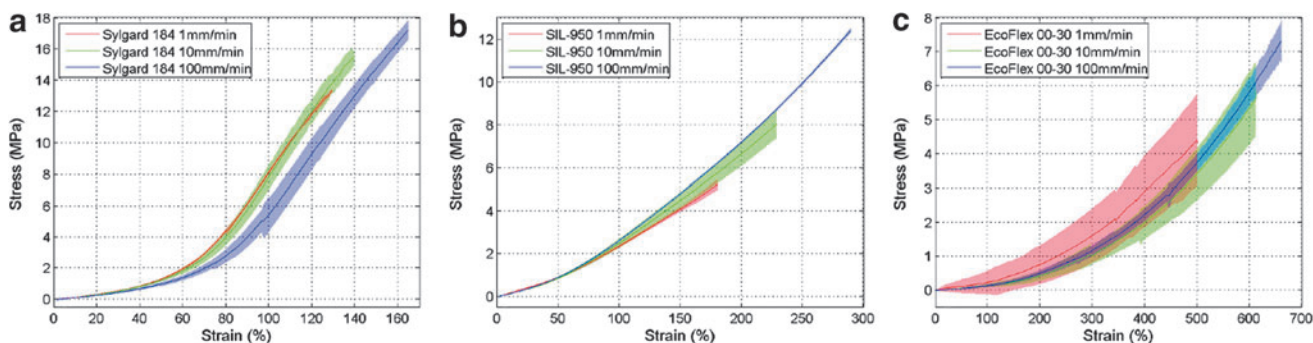


FIG. 3. Pull-to-failure data for (a) Sylgard 184, (b) Smooth-Sil 950, and (c) EcoFlex 00-30 with 95% confidence interval (shaded region).

Material testing was conducted using an Instron 3345 single-column material tester fitted with a 1 kN load cell using custom-made material grips. We conducted a preliminary series of tests to determine the extension correction factor to convert between applied extension and the actual extension observed within the elastomeric material. In the case of the material test samples, we applied two small black ink dots to the elastomeric sample as shown in Figure 2. We then placed the sample in the Instron and measured the distance between the dots using a digital calipers at approximately 0%, 20%, 40%, 60%, and 80% of the extension at failure. In the case of the resistive strain gauge samples, we measured length from 0 to 35 mm extension in 5 mm increments. We limited the strain in the resistive strain sensors due to electrical failure at higher strains. In both cases, we assumed a linear relation between extension and gauge length. For EcoFlex 00-30, these correction factors (for the material test dog bone and resistive strain sensor) were $L = 25.4 + 0.538E$ and $L = 24.5 + 0.709E$, for Sylgard 184 the factors were $L = 25.4 + 0.515E$ and $L = 25.8 + 0.550E$, and for Smooth-Sil 950 the factors were $L = 25.4 + 0.580E$ and $L = 26.2 + 0.597E$, where L is the gauge length, and E is the extension. These correction factors were used for all subsequent tests. Although this method is not as accurate as measuring gauge factors for each test, we believe it is sufficiently

accurate to support our objective of providing qualitative assessment of material properties.

Our tests included five types of tests using three methods, which are pull-to-failure tests, cyclic loading tests, and stress relaxation tests. Within the first method, we conducted three types of tests: variable strain rate tests, batch-to-batch consistency tests, and prestrain tests. Cyclic loading and stress relaxation tests were performed on the strain sensors to determine their resistive response in both of these loading modes. Each test was run three times for each elastomer, with the exception of the cyclic loading tests. The average and 95% confidence interval for the experiment was determined based on the data obtained in each of the three runs.

Pull-to-failure: variable strain rate

Our first series of tests involved pulling samples at a constant rate until failure. We peeled the cured samples off of the substrates and placed the samples directly into the sample holders. We measured the stress and strain of all three elastomer types at strain rates of 1, 10, and 100 mm/min. The stress-strain curves for various strain rates for Sylgard 184, Smooth-Sil 950, and EcoFlex 00-30 are shown in Figure 3. All three elastomers are shown on a common axis for comparison in Figure 4.

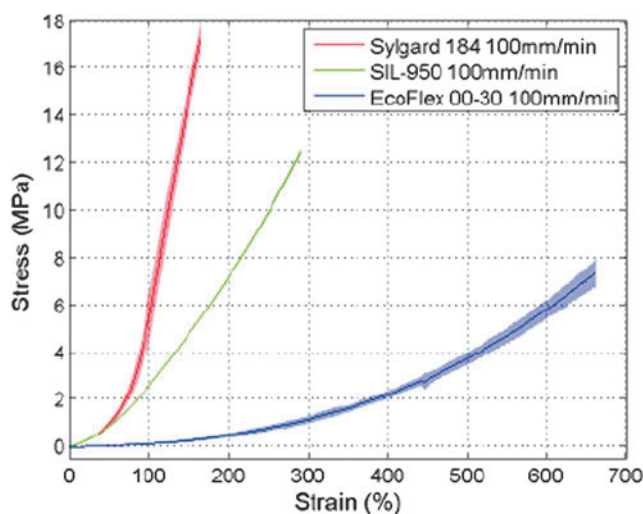


FIG. 4. Pull-to-failure data for each material at 100 mm/min. Shaded areas represent 95% confidence intervals.

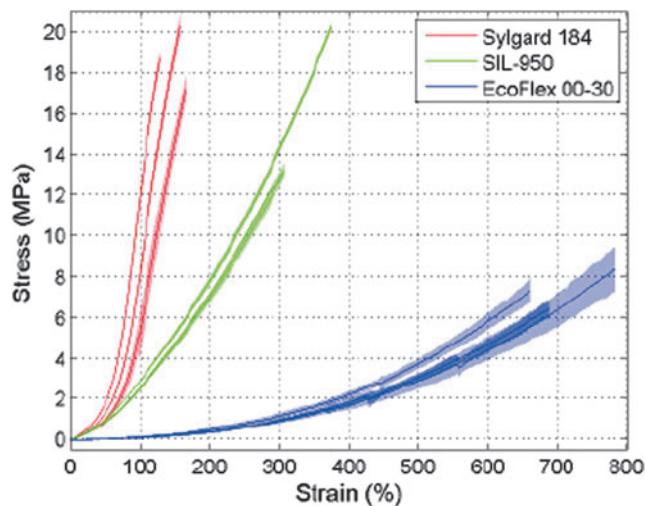


FIG. 5. Pull-to-failure data for each material at 100 mm/min of three separate batches. Shaded areas represent 95% confidence intervals.

Pull-to-failure: batch-to-batch consistency

To determine batch-to-batch consistency between the materials, three batches of each elastomer were made over a 20-day period. Samples from all batches were pulled at a strain rate of 100 mm/min. The results of these tests are shown in Figure 5. These samples were prepared using common laboratory equipment, and we believe they represent the level of variability that would be expected in practice.

Pull-to-failure: effect of prestrain

To determine the effect of prestrain, we removed a sample from the glass substrate on which it was cured, prestrained the sample to approximately 80% of the failure extension, and then relaxed it either briefly or overnight. In both cases, we completely removed the sample from the test fixture. After replacing the sample in the fixture, the sample was pulled to failure at a rate of 100 mm/min. The results for Sylgard 184, Smooth-Sil 950, and EcoFlex 00-30 are shown in Figure 6.

Cyclic loading tests

Our cyclic loading tests were designed to analyze the response of elastomers in conditions representative of what might be experienced in a robotic application. We extended the samples at fixed rates of 10 and 100 mm/min to approximately 80% of the failure extension, and then returned at the same rate to 0 mm extension, repeating this process for 10 cycles. Cyclic loading tests were performed on strain sensors to capture repeatability. The sensors were cycled between 0 mm to an absolute extension of 32 mm for 10 cycles. The stress–strain curves of tests for the Sylgard 184, Smooth-Sil 950, and EcoFlex 00-30 are shown in Figure 7a–c. The resistive sensor results of these tests for Sylgard 184, Smooth-Sil 950, and EcoFlex 00-30 are shown in Figure 7d–f.

Stress relaxation tests

Our final series of tests were designed to capture the long-duration stress relaxation behavior of these elastomers. We applied an extension of approximately 80% of the failure extension at a rate of 1,000 mm/min, and held the extension for 3 h. For strain sensors, we applied an absolute extension of 32 mm at a rate of 1,000 mm/min and held for 3 h. Material stress relaxation curves for each material are shown in Figure 8a. The curves for the resistive sensors' stress relaxation tests are shown in Figure 8b.

Results and Discussion

Material properties are dependent on strain rate

Material properties are typically thought of as strain rate invariant. However, our experiments show that this is not a valid assumption in the case of these elastomers. From Figure 3, we can see that the stress–strain relationship is dependent on strain rate. In the case of Sylgard 184 (Fig. 3a), we see that at 100 mm/min, the material becomes softer than at 1 or 10 mm/min. Smooth-Sil 950 (Fig. 3b) shows increasing stiffness with increasing strain rate, an opposite effect from Sylgard 184. EcoFlex 00-30 (Fig. 3c) generally shows softening with increasing strain rates, but the wide confidence intervals prevent any definitive conclusions. We believe that the range between 1 and 100 mm/min is representative of soft

robotic applications such as a strain gauge positioned on a manipulator joint for proprioceptive sensing. Without accounting for the effects of strain rate dependence, using a nominal Young's modulus for these elastomers would give erroneous results.

Material properties are sensitive to production variations

From a practical standpoint, the soft robotics researcher should be concerned about the variability of material properties between batches. Our experiments have shown that, even with what we consider practical process control over small batches, we see a meaningful difference in material properties between batches. Figure 5 shows the stress–strain relationships for three nominally identical batches for each of our three test materials. Sylgard 184 shows the most variation. For example, at 100% strain, the stress varies from 5.5 to 12.0 MPa. The curves also demonstrate the small confidence intervals within a batch, suggesting that batches are internally consistent, and that samples taken from the same batch exhibit similar material properties. We believe that these variations are a significant contributor to the variation in the published data. For this reason, we suggest that nominal material values are not sufficient in critical applications. Instead, materials should be measured once fabricated to ensure that accurate material properties are known.

Initial strain results in irreversible material changes

Another significant finding is that material properties change irreversibly after initial strain, a confirmation that the Mullins effect is present in these materials. This is clearly illustrated in Figure 6. Of the three materials tested, Smooth-Sil 950 (Fig. 6b) and EcoFlex 00-30 (Fig. 6c) exhibited the most pronounced change in stiffness, while Sylgard 184 (Fig. 6a) exhibited the same effect to a lesser degree. In these materials, straining and relaxing the material had the effect of reducing its stiffness in the middle of the extension regime. As strain increases to yield, the stiffness of the prestrained material quickly increases to match that of the native samples. In the most extreme case, Smooth-Sil 950 shows a 40% reduction in stiffness at 200% strain. There are significant differences in stiffness in Smooth-Sil 950 from nearly 0% strain to 250% strain. In Sylgard 184, the effected region is from 60% to 120%, and in EcoFlex 00-30, it is from 100% to 500% strain. We also note that, in the case of Smooth-Sil 950, the material becomes considerably more nonlinear once it has gone through an initial strain cycle. Sylgard 184 and EcoFlex 00-30 are already sufficiently nonlinear that the qualitative changes in behavior are less pronounced. Since most soft robotic applications operate in the middle of the elastic strain regime, where this prestrain effect is most pronounced, we conclude that this is an important effect that needs to be considered by soft robotics designers and by those groups measuring material properties for soft robotics applications.

Cyclic loading tests show an absence of work hardening

The cyclic loading tests shown in Figures 7a–c show three effects. First, they confirm the results of the prestrain tests discussed above, and show that there is a significant change in

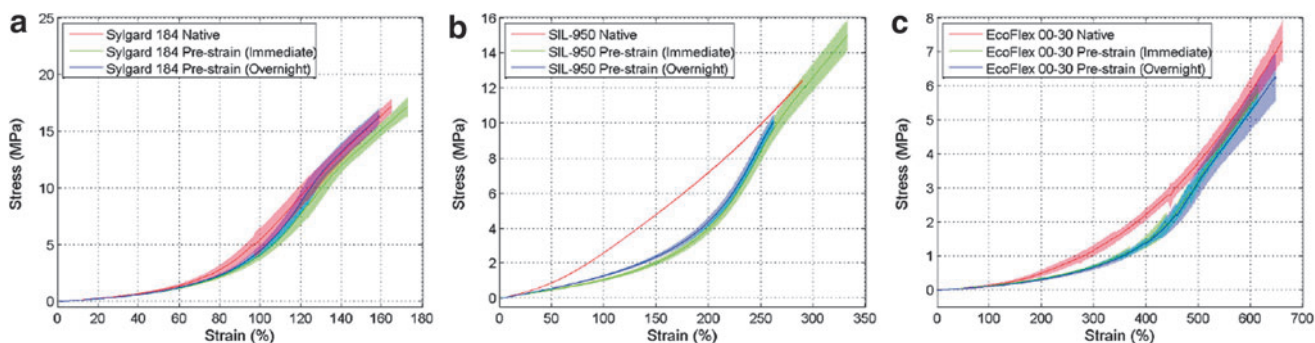


FIG. 6. Pull-to-failure data for (a) Sylgard 184, (b) Smooth-Sil 950, and (c) EcoFlex 00-30 with prestrained samples. Shaded areas represent 95% confidence intervals.

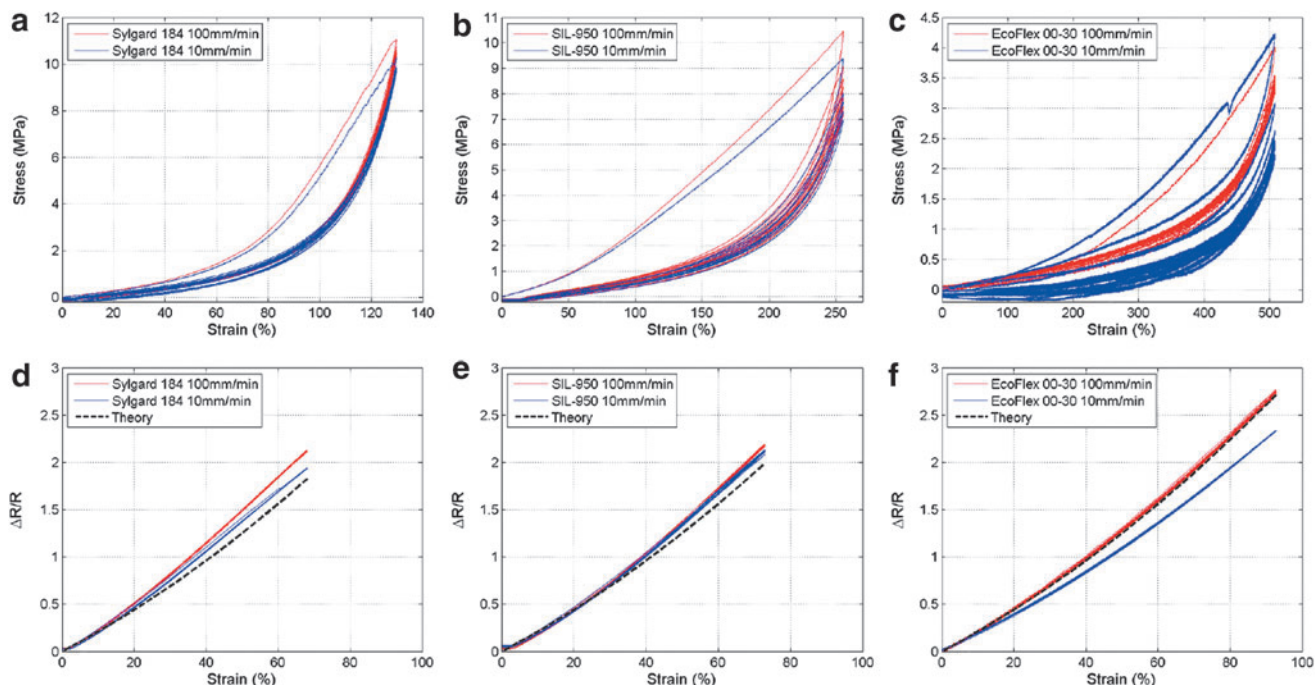


FIG. 7. Material cyclic loading tests for (a) Sylgard 184, (b) Smooth-Sil 950, and (c) EcoFlex 00-30 and resistive strain cyclic loading tests for (d) Sylgard 184, (e) Smooth-Sil 950, and (f) EcoFlex 00-30. Data are for 10 complete cycles. Jumps in the data are due to slipping of the sample during the course of the test.

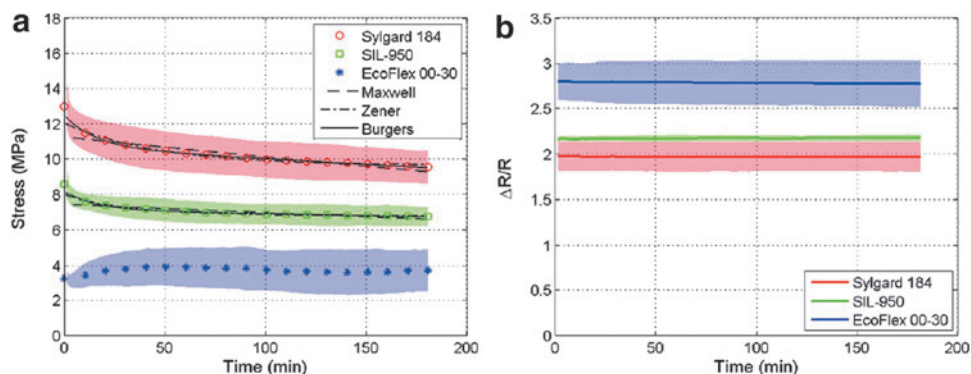


FIG. 8. (a) Step extension response for Sylgard 184, Smooth-Sil 950, and EcoFlex 00-30. Shaded areas represent 95% confidence intervals of the experimental data, the markers represent the averaged experimental data, and the black lines represent the theoretical models: Maxwell, Zener, and Burgers. (b) Step extension response for Sylgard 184, Smooth-Sil 950, and EcoFlex 00-30 strain sensors. Shaded areas represent 95% confidence intervals.

material properties after the first loading cycle. Second, they show that no significant changes in material properties take place during the subsequent 10 loading cycles, as all of the subsequent data fall within a narrow band. Third, the figures show that there is little to no mechanical hysteresis observed in the materials at these loading rates, since the loading and unloading traces fall over one another. In the case of EcoFlex 00-30 (Fig. 7c), the variation in data arises from a low-frequency noise source. However, the qualitative results from EcoFlex 00-30 match the other two materials.

Stress relaxation behaviors are well-modeled by the Burgers model

Both the Zener and the Burgers models for viscoelastic stress relaxation show good agreement with Sylgard 184 and Smooth-Sil 950 experimental data. Figure 8a shows the 95% confidence intervals for the long-duration creep tests of the three materials, and the Maxwell, Zener, and Burgers models fit for Sylgard 184 and Smooth-Sil 950. We were unable to fit a model to the EcoFlex 00-30 data, due to significant low-frequency noise. Our hypothesis is that this error is thermal in nature, and is either due to time-varying heating of the material, the load cell, or a combination of the two. We fit Equations 2–4 to the observed stress data using a least-squares regression. From the data, we can see that a two-element model (Maxwell) is not sufficient to capture the transient dynamics of the material. The three-element model (Zener) is better able to capture the “slow” transient dynamics, but still is unable to capture the “fast” transient. The four-element model (Burgers) captures both the “fast” and “slow” transient effects. That behavior can be seen in Figure 8a, which shows a short, fast creep stage ($t < 25$ min), followed by a slower creep stage.

Strain gauge measurements are highly repeatable

Across all of the materials, the resistance response to strain is highly consistent and repeatable with no visible Mullins effect. Further, we find that the resistance response of the strain gauge is well-modeled by the simple analytical model developed in Equation 8. Moreover, since the analytical model contains no fitting parameters or arbitrary coefficients, we do not have to fit the model to the experimental data. Although the material response in terms of stress versus strain exhibits a higher-order nonlinearity, the normalized resistance change versus strain response exhibits only a quadratic effect, as predicted by the model. The results of normalized resistance change versus strain are shown in Figures 7d–f. We conclude from these measurements that embedded liquid-metal-resistive strain gauges are an appropriate sensing modality for proprioception in soft robotic systems.

Strain gauges are not susceptible to material viscoelastic stress relaxation

The long-term response of the strain gauge resistance measurements shows little to no effect of stress relaxation. This is predicted by Equation 8, which shows that there should be no correlation between stress in the material and the output resistance. Although the stress in the elastomer is changing over time, the strain remains fixed, and hence the resistance is unchanged. The results of these long-duration

tests are shown in Figure 8b. This result supports our conclusion that embedded liquid metal sensors are appropriate for soft robotic proprioception, as they respond to the current strain state without regard for previous strain states.

Conclusions

Our experiments have examined three elastomers that have been used in soft robotic applications. Our focus has been on identifying material properties that are of concern to the designer of soft robotic systems. Models for these properties have been developed by Ogden and Simo and Hughes, but require experimental data to determine the coefficients for a particular material. This work begins to fill the void present in the literature with regard to soft material properties. The elastomeric materials discussed in this article are very different from metals, and many of the simplifying assumptions that can be made with small deformations are no longer applicable when discussing finite deformations of viscoelastic materials. Instead, richer dynamics must be evaluated, as demonstrated by the experimental results we have presented. We believe that the work presented here will be useful in the design of conformable electronics, soft actuators, active wearable systems, sensory skins, and other highly deformable robotic systems.

Our experiments also validated the use of embedded liquid metal strain sensors in soft robotic applications. These devices show good correlation between their output and their current strain state, without significant effect from the material properties of the elastomeric substrate. This is in good agreement with the simple analytical model developed for these devices. In actual soft robotic applications, our experimental results demonstrate that strain gauges can be used to provide proprioception.

Acknowledgments

E.L.W. is supported under the National Science Foundation Graduate Research Fellowship program (DGE-1333468). This work was partially supported by an Early Career Faculty grant from NASA’s Space Technology Research Grants Program (NNX14A052G).

Disclaimer

Any opinions, findings, and conclusions or recommendations expressed in this article are those of the authors and do not necessarily reflect the views of the National Science Foundation or the National Aeronautics and Space Administration.

Author Disclosure Statement

The authors declare that they have no competing financial or other interests that present a conflict of interest.

References

1. Park Y-L, Chen B-R, Wood RJ. Design and fabrication of soft artificial skin using embedded microchannels and liquid conductors. *IEEE Sens J* 2012;12:2711–2718.
2. Chossat JB, Park Y-L, Wood RJ. A soft strain sensor based on ionic and metal liquids. *IEEE Sens J* 2013;13:3405–3414.
3. Menguc Y, Park Y-L, Martinez-Villapando E, *et al.* Soft wearable motion sensing suit for lower limb biomechanics

- measurements. 2013 IEEE International Conference on Robotics and Automation (ICRA), 2013, pp. 5309–5316.
4. Kramer RK, Majidi C, Wood RJ. Wearable tactile keypad with stretchable artificial skin. 2011 IEEE International Conference on Robotics and Automation (ICRA), 2011, pp. 1103–1107.
 5. Lee H-K, Chang S-I, Yoon E. Dual-mode capacitive proximity sensor for robot application: implementation of tactile and proximity sensing capability on a single polymer platform using shared electrodes. *IEEE Sens J* 2009;9:1748–1755.
 6. Cotton DPJ, Graz IM, Lacour SP. A multifunctional capacitive sensor for stretchable electronic skins. *IEEE Sens J* 2009;9:2008–2009.
 7. Fassler A, Majidi C. Soft-matter capacitors and inductors for hyperelastic strain sensing and stretchable electronics. *Smart Mater Struct* 2013;22:055023.
 8. Wei W, Guo S. A novel PDMS diaphragm micropump based on ICPF actuator. 2010 IEEE International Conference on Robotics and Biomimetics (ROBIO), 2010, pp. 1577–1583.
 9. Cho MS, Seo HJ, Nam JD, *et al.* An electroactive conducting polymer actuator based on NBR/RTIL solid polymer electrolyte. *Smart Mater Struct* 2007;16:S237.
 10. Bahramzadeh Y, Shahinpoor M. A review of ionic polymeric soft actuators and sensors. *Soft Robotics* 2014;1:38–52.
 11. Shepherd RF, Ilievski F, Choi W, *et al.* Multigait soft robot. *PNAS* 2011;108:20400–20403.
 12. Suzumori K, Endo S, Kanda T, *et al.* A bending pneumatic rubber actuator realizing soft-bodied manta swimming robot. 2007 IEEE International Conference on Robotics and Automation, 2007, pp. 4975–4980.
 13. Polygerinos P, Wang Z, Galloway KC, *et al.* Soft robotic glove for combined assistance and at-home rehabilitation. *Robotics Auton Syst* 2014; in press.
 14. Martinez RV, Branch JL, Fish CR, *et al.* Robotic tentacles with three-dimensional mobility based on flexible elastomers. *Adv Mater* 2013;25:205–212.
 15. Cianchetti M, Mattoli V, Mazzolai B, *et al.* A new design methodology of electrostrictive actuators for bio-inspired robotics. *Sens Actuat B Chem* 2009;142:288–297.
 16. Pelrine R, Kornbluh RD, Pei Q, *et al.* Dielectric elastomer artificial muscle actuators: toward biomimetic motion. SPIE's 9th Annual International Symposium on Smart Structures and Materials, 2002, pp. 126–137.
 17. Madden JD, Vandesteeg NA, Anquetil PA, *et al.* Artificial muscle technology: physical principles and naval prospects. *IEEE J Ocean Eng* 2004;29:706–728.
 18. Boley JW, White EL, Chiu GTC, Kramer RK. Direct writing of gallium indium alloy for stretchable electronics. *Adv Funct Mater* 2014;24:3501–3507.
 19. Majidi C, Kramer R, Wood RJ. A non-differential elastomer curvature sensor for softer-than-skin electronics, *Smart Mater Struct* 2011;20:105017.
 20. Kramer RK, Majidi C, Sahai R, Wood RJ. Soft curvature sensors for joint angle proprioception. 2011 IEEE/RSJ International Conference on Intelligent Robots and Systems (IROS), 2011, pp. 1919–1926.
 21. Hammond FL, Kramer RK, Wan Q, *et al.* Soft tactile sensor arrays for micromanipulation. 2012 IEEE/RSJ International Conference on Intelligent Robots and Systems (IROS), 2012, pp. 25–32.
 22. Ogden RW. *Non-Linear Elastic Deformations*. Dover Publications: 1997.
 23. Simo JC, Hughes TJR. *Computational Inelasticity*. Springer: 2008.
 24. Saccomandi G, R. W. Ogden. *Mechanics and Thermo-mechanics of Rubberlike Solids*. New York, NY; Springer: 2004.
 25. Ogden RW, Saccomandi G, Sgura I. Fitting hyperelastic models to experimental data. *Comput Mech* 2004;34:484–502.
 26. Ogden RW. *Nonlinear Elasticity with Application to Material Modelling*. In: AMAS Lecture Notes, Vol. 6, Warsaw, Poland, 2003.
 27. Dorfmann A, Ogden RW. A pseudo-elastic model for loading, partial unloading and reloading of particle-reinforced rubber. *Int J Solids Struct* 2003;40:2699–2714.
 28. Ogden RW, Holzapfel GA. *Mechanics of Biological Tissue*. Springer, 2006.
 29. Overvelde JT, Menguc Y, Polygerinos P, *et al.* Numerical mechanical and electrical analysis of soft liquid-embedded deformation sensors. *Extreme Mech Lett* 2014;1:42–46.
 30. Schneider F, Fellner T, Wilde J, Wallrabe U. Mechanical properties of silicones for MEMS. *J Micromech Microeng* 2008;18:065008.
 31. Kim TK, Kim JK, Jeong OC. Measurement of nonlinear mechanical properties of PDMS elastomer. *Microelectron Eng* 2011;88:1982–1985.
 32. Mullins L. Effect of stretching on the properties of rubber. *Rubber Chem Technol* 1948;21:281–300.
 33. Diani J, Fayolle B, Gilormini P. A review on the Mullins effect. *Eur Polym J* 2009;45:601–612.
 34. Findley WN. *Creep and Relaxation of Nonlinear Viscoelastic Materials: With an Introduction to Linear Viscoelasticity*. New York: Dover, 1989.
 35. McCrum NG, Buckley CP, Bucknall CB. *Principles of Polymer Engineering*. New York: Oxford University Press, 1997.
 36. Meng E, Zhang X, Benard W. Additive Processes for Polymeric Materials. In: *MEMS Materials and Processes Handbook*. New York: Springer, 2011, pp. 198–271.
 37. Hyun-Joong K, Son C, Ziaie B. A multiaxial stretchable interconnect using liquid-alloy-filled elastomeric microchannels. *Appl Phys Lett* 2008;92.

Address correspondence to:

Rebecca K. Kramer
 Department of Mechanical Engineering
 Purdue University
 585 Purdue Mall, ME 2147
 West Lafayette, IN 47907

E-mail: rebeccakramer@purdue.edu